# Complexity of Lipid Domains and Rafts in Giant Unilamellar Vesicles Revealed by Combining Imaging and Microscopic and Macroscopic Time-Resolved Fluorescence

Rodrigo F. M. de Almeida,*†‡ JanWillem Borst,* Alexander Fedorov,‡ Manuel Prieto,‡ and Antonie J. W. G. Visser*

*MicroSpectroscopy Centre, Laboratory of Biochemistry, Wageningen University, Wageningen, The Netherlands; †Centro de Química e Bioquímica, Faculdade de Ciências da Universidade de Lisboa, Lisbon, Portugal; and ‡Centro de Química-Física Molecular, Instituto Superior Técnico da Universidade Técnica de Lisboa, Lisbon, Portugal

ABSTRACT The application of fluorescence lifetime imaging microscopy to study gel/fluid and raftlike lipid domains in giant unilamellar vesicles (GUVs) is demonstrated here. Different regions of the ternary dipalmitoylphosphatidylcholine/dioleoylphosphatidylcholine/cholesterol phase diagram were studied. The head-labeled phospholipid Rhodamine-dioleoylphosphatidylethanolamine (Rhod-DOPE) was used as a fluorescent probe. Gel/fluid and liquid-ordered ($l_o$)/liquid-disordered ($l_d$) phase separation were clearly visualized upon two-photon excitation. Fluorescence intensity decays in different regions of a GUV were also obtained with the microscope in fixed laser-beam configuration. The ensemble behavior of the system was studied by obtaining fluorescence intensity decays of Rhod-DOPE in nongiant vesicle suspensions. The fingerprints for gel/fluid coexistence and for the presence of $l_o$ raftlike phase, based on fluorescence lifetime imaging microscopy histograms and images, and on the fluorescence intensity decay parameters of Rhod-DOPE, are presented. The presence of three lipid phases in one single GUV is detected unequivocally. From the comparison of lifetime parameters, it can be concluded that the $l_o$ phase is formed in the binary dipalmitoylphosphatidylcholine/cholesterol but not in the dioleoylphosphatidylcholine/cholesterol mixture. The domains apparent in fluorescence intensity images have a more complex substructure revealed by analysis of the lifetime data. The potential applications of this combined imaging/microscopic/macroscopic methodology are discussed.

## INTRODUCTION

The paradigm of biomembranes has shifted from the fluid mosaic model to a domain mosaic, where a lateral organization in different length scales is patent (1,2). The lateral membrane domains can have different physical origins and include differential lipid-lipid interactions (3,4). In this respect, the study of lipid mixtures in membrane model systems has been crucial to understand the formation of lipid domains in biological membranes (5,6). However, even in simple model systems, the lateral lipid heterogeneity is not a simple issue, and controversy persists when comparing results from different techniques (7). From spectroscopic and calorimetric bulk techniques, the macrothermodynamic behavior of the system can be appreciated and complete phase diagrams can be built (8). These diagrams can also be used as the basis for further detailed studies, using Förster's resonance energy transfer (FRET) and microscopy, for example, to address questions like the size and the shape of domains in clearly defined regions of the phase diagram (9,10). Fluorescence microscopy has also been used to obtain lipid phase diagrams (11,12). However, the direct detection of three phase-coexistence is very troublesome and when the heterogeneities are of submicron scale they cannot be readily detected (13). This can happen when the amount of one of the phases is very small. It can also be due to the characteristics of the lipid system itself, because lipids with intermediate configurations located at the domain interfaces can reduce the interfacial tension preventing domain growth (14).

Nevertheless, the fact that microscopic techniques allow for direct observation of gel/liquid-disordered ($l_d$) (15) and liquid-ordered ($l_o$) raftlike (16) heterogeneities has made them very attractive. Also due to the resemblance of giant unilamellar vesicles (GUVs) to cell membranes in terms of size, their use has been increasingly more important. In this way, the use of more sophisticated microscopic approaches, where spectroscopic data is combined with direct visualization (imaging) of the lipid bilayer have become indispensable (e.g., the use of generalized polarization (GP) of Laurdan (16), or of fluorescence correlation spectroscopy (FCS) (17,18) and, more recently, an interesting combination of fluorescence microscopy and NMR (19)). In addition, very recently, ceramide domains have been elegantly investigated in a study combining FCS, AFM, and confocal fluorescence microscopy (20) and in another one exploiting confocal and two-photon fluorescence microscopy of GUVs, and multilamellar vesicles (MLVs) data with Laurdan GP and infrared spectroscopy (21).

In the present study, we apply for the first time a combined time-resolved fluorescence microspectroscopic approach, i.e.,

1. Fluorescence lifetime imaging microscopy (FLIM) in which laser scanning microscopy is combined with fluorescence

*Submitted October 3, 2006, and accepted for publication March 21, 2007.*

Address reprint requests to Rodrigo F. M. de Almeida, E-mail: r.almeida@mail.ist.utl.pt.

Editor: Akihiro Kusumi.



0006-3495/07/07/539/15 $2.00

doi: 10.1529/biophysj.106.098822

decay acquisition over a section of a GUV; this methodology yields spatial resolution, but low photon counts in each decay (pixel), and thus poorer statistics.
2. Microscopic fluorescence decays, in which the laser is focused in a chosen position on a GUV and a high-count number decay is acquired under the microscope, returning mainly the fluorescence of a specific region of a GUV.
3. Macroscopic decays in MLV or large unilamellar vesicle (LUV) suspensions, which reveal the ensemble behavior of the system, and in which high count number decays are also retrieved. This combined approach is used to study lateral lipid heterogeneity in a raft-mimicking ternary mixture of an unsaturated phospholipid (1,2-dioleoyl-*sn*-glycero-3-phosphocholine, DOPC), a saturated phospholipid (1,2-dipalmitoyl-*sn*-glycero-3-phosphocholine, DPPC), and cholesterol.

This system is most adequate for the establishment of the potentialities and limitations of the techniques used in this study. The phase behavior of the binary mixtures DOPC/DPPC (22,23) and DPPC/cholesterol (24–26) has been studied both theoretically and experimentally, and in addition, it is consensual that at room temperature there is no formation of $l_o$ phase in mixtures of DOPC and cholesterol, whereas there is gel/$l_o$ phase coexistence for DPPC/cholesterol at this temperature (19). Moreover, fluorescence microscopy studies have been performed for the DOPC/DPPC/cholesterol mixture (together with NMR, (27); and FCS, (28)).

The fluorescent probe *N*-(lyssamine Rhodamine B sulfonyl)-dioleoylphosphatidylethanolamine (Rhod-DOPE) was chosen because:

1. It is a head-labeled phospholipid, thus with minimal perturbation on the bilayer.
2. Its emission is in the visible range.
3. It has high photostability.
4. It can be used for detection of lipid domains by two-photon microscopy (29).
5. It was characterized in the raft palmitoylsphingomyelin (PSM)/palmitoyloleoylphosphatidylcholine (POPC)/cholesterol system showing a fluorescence lifetime that is sensitive to the presence of lipid rafts (9).

The approach used in this study shows potential in improving our understanding of the structure, dynamics, and composition of lipid domains and rafts. Through the application of a stepwise methodology, evidence for, e.g., three-phase coexistence and for submicrometer structure of imaged domains was obtained.

## MATERIALS AND METHODS

### Chemicals

DOPC, DPPC, and Rhod-DOPE were purchased from Avanti Polar Lipids (Birmingham, AL). Cholesterol was purchased from Sigma (St. Louis, MO). All other reagents were of the highest purity available.

### Vesicle preparation

MLVs containing the appropriate lipids and Rhod-PE when used were prepared by standard procedures. Briefly, adequate volumes of lipids and probe stock solutions were added to a tube to have the desired lipid mole fractions and lipid/probe ratio. The solvent was slowly vaporized by a mild flow of nitrogen, forming a thin layer of lipid in the bottom of the tube. The lipid was hydrated by addition of 1 ml of MilliQ water (Millipore, Billerica, MA) previously heated above the $T_m$ of DPPC. The samples were then progressively vortex-stirred and submitted to freeze/thaw cycles (liquid nitrogen/water bath at 60°C). Afterwards, they were slowly cooled and kept in the dark at 4°C. Before measurements, they were slowly brought to room temperature. The suspension medium was MilliQ purified water (>18 MΩ; <5 ppb). The probe/lipid ratio used was 1:500. Total lipid was 0.5 mM. As a consequence of the preparation procedure, the probe is evenly distributed among the two bilayer leaflets. To ensure that multilamellarity was not influencing the results, the measurements were repeated in large unilamellar vesicle (LUV) suspension for several compositions in different regions of the phase diagram. LUVs were obtained by the extrusion method (30). Briefly, the MLV suspension obtained as described above was forced through a pair of polycarbonate filters with pore diameter of 0.1 $\mu$m 21 times, in an Avanti Mini-Extruder (Avanti Polar Lipids).

GUVs were prepared by the electroformation method ((31); see also (32,33)). Briefly, adequate volumes of lipids and probe stock solutions were added to a tube to have the desired lipid mole fractions and lipid/probe ratio, a final lipid concentration of ~1 mM, and a chloroform/methanol ratio of ~2:1 (v/v), because these conditions were shown to be optimal for GUV growth in our system. The mixture was homogenized by vortexing, and 0.5 $\mu$l of solution was spread on each side of the flattened tip of a pair of Pt wires with a gas-tight syringe. The traces of organic solvent were removed through vacuum desiccation. The Pt wires are soldered to a thicker Ag wire in order to be hanging in parallel positions, connected to the signal generator, and inserted in a tube. A sinusoidal signal with a peak-to-peak voltage of 0.2 V and 10 Hz was applied. The samples were gently hydrated with 1.0 ml of 200 mM sucrose solution in MilliQ water, and the voltage was increased to 2.0 V and maintained for 90–120 min. Then, the frequency was decreased to 0.5 Hz, the voltage to 0.2 V, and finally the signal generator turned off. In case of DPPC-containing mixtures, the tubes were in a block heater at 60°C, and the sucrose solution was previously heated to that temperature. The Pt wires were taken from the tubes, releasing the nonoxidized GUVs into the sucrose solution. The vesicle suspension was kept at room temperature (24°C) in the dark until use.

DPPC and DOPC concentration in stock solutions (chloroform) were confirmed by phosphorus analysis (34). Probe concentrations were determined spectrophotometrically: $\varepsilon$(Rhod-PE, $\lambda_{max} = 559$, chloroform) $= 95 \times 10^3$ $M^{-1}$ $cm^{-1}$ (35). Cholesterol concentration in stock solutions was determined by gravimetry.

### FLIM and microscopic decays on GUVs

An aliquot (~100 $\mu$l) of GUV suspension was added to a chamber of an eight-well plastic plate with glass-like coverslip bottom. Then, a similar volume of an equiosmolar glucose solution (200 mM) was added. Due to the density difference between the final external solution, and the solution inside the vesicles, the GUVs precipitate in the bottom of the chamber, facilitating the observation in the inverted microscope (36).

Fluorescence lifetime imaging microscopy (FLIM), e.g., (37), was performed using a Bio-Rad Radiance 2100 MP system (Hercules, CA) in combination with a Nikon TE 300 inverted microscope (Tokyo, Japan). 860 nm 2-photon excitation (TPE) was used to excite Rhod-DOPE. TPE pulses were generated by a Ti:Sapphire Mira laser (Coherent Laser, Santa Clara, CA) that was pumped by a 5 W Coherent Verdi laser. Pulse trains of 80 MHz (150 fs pulse duration, 860 nm center wavelength) were produced. The excitation light was directly coupled into the microscope and focused into the sample using a CFI Plan Apochromat 60× water immersion objective

lens (numerical aperture 1.2, Nikon). Fluorescence emission was detected using the non-descanned single photon-counting technique. For this purpose, a model No. R3809U MCP photomultiplier tube (Hamamatsu, Hamamatsu City, Japan) with a typical time resolution of ~50 ps was used as a detector. The emission light was selected with a 620DF60 band-pass filter for time-resolved acquisitions. Images with a frame size of 64 × 64 pixels were acquired using a Becker and Hickl (Berlin, Germany) SPC 830 module (38). Typically, under these conditions the average count rate was ~2–3 × $10^4$ counts/s and 90 s scanning time was used for image acquisition (39). The acquisition time was set to a maximum of 2 min in cases where the count rate was slightly lower. In many experiments the count rate was higher (~4 × $10^4$ counts/s; usually higher count rates correspond to bigger GUVs). Complete fluorescence intensity decays were calculated for each nine pixels (one central pixel and the eight surrounding pixels in a square lattice), and either a single exponential or a biexponential model was fitted using the Becker and Hickl software. The fit procedure could be improved if the offset were selected manually by choosing the appropriate channels; in addition, the number of maximum iterations was increased until no significant changes in the $\chi^2$ and lifetime histograms was observed by further cycles. The histogram gives the pixel distribution of a certain analysis parameter. The image can be plotted in a false color code associated to this parameter distribution. In case of the lifetime histogram, the frequency is intensity-weighted, i.e., pixels with higher total number of photons have a stronger contribution to the histogram because they are statistically more meaningful. This color code is then used to reconstruct a lifetime image. To obtain high count number decays, similar to ensemble (vesicle suspension) macroscopic decays, the laser beam was fixed during acquisition in the center of an operator-selected rectangular region of interest, and all the emission photons were collected during 30–90 s (microscopic decays). After the acquisition, a background-decay was obtained with the same accumulation time, but with the laser fixed outside the vesicle. The high count number microscopic decays were analyzed using the TRFA software (Scientific Software Technologies Center, Minsk, Belarus) based on the Marquardt algorithm.

### Time-resolved fluorescence spectroscopy on MLV and LUV suspensions

For ensemble measurements in MLV (or LUV) suspensions, the instrumentation (single-photon timing technique) consisted of a cavity-dumped dye laser of Rhodamine 6G, synchronously pumped by a mode-locked $Ar^+$ laser (514.5 nm, Coherent Innova 200-10). Rhod-DOPE emission was measured at $\lambda = 620$ nm using the magic angle (54.7°) relative to the vertically polarized excitation beam ($\lambda = 575$ nm) using a Hamamatsu R-2809 MCP photomultiplier. The instrument response functions (~80 ps full width half-maximum) for deconvolution were generated from scatter dispersion of colloidal silica in water (Aldrich, Milwaukee, WI). The fluorescence decays were obtained with an accumulation of 20,000 counts in the peak channel, and timescales ranging from 7.5 ps/channel to 15.3 ps/channel were used. The fluorescence quartz cells had 0.5 cm × 0.5 cm dimensions.

For a fluorescence intensity decay described by the sum of two exponentials, i.e.,

$$i(t) = \alpha_1 \exp(-t/\tau_1) + \alpha_2 \exp(-t/\tau_2), \quad (1)$$

where $\alpha_1$ and $\alpha_2$ are the normalized amplitudes, and $\tau_1$ and $\tau_2$ are the lifetimes associated to components 1 and 2 of the fluorescence decay, the mean or average lifetime is given by

$$\langle\tau\rangle = (\alpha_1\tau_1^2 + \alpha_2\tau_2^2)/(\alpha_1\tau_1 + \alpha_2\tau_2), \quad (2)$$

and the amplitude-weighted lifetime or lifetime-weighted quantum yield is defined as

$$\bar{\tau} = \alpha_1\tau_1 + \alpha_2\tau_2 \quad (3)$$

(e.g., (8)).

## RESULTS

### DOPC, DPPC, and DPPC/DOPC binary mixtures

The fluorescence intensity and lifetime images of Rhod-DOPE in a pure DOPC GUV and in a pure DPPC MLV show an homogenous appearance (Fig. 1, *A*, *B*, *D*, and *E*). This pattern is reflected in the lifetime histograms (Fig. 1, *C* and *F*, respectively), that have only a sharp peak at ~2.7 ns for DOPC (fluid) and 2.6 ns for DPPC (gel). As will be shown later, the same lifetime histogram is obtained for DOPC MLVs and DPPC GUVs. Thus, the probe displays the same behavior in each of those two pure phases. This is corroborated by the microscopic decays (Table 1). For both lipid systems, a monoexponential decay with the same fluorescence lifetime corresponding to the peak in the FLIM lifetime histogram is obtained, regardless of the focal spot of the laser (equatorial, polar, or intermediate). Finally, in case of macroscopic, MLV (LUV) suspensions, fluorescence decays for the same lipid compositions (Table 2) show a multiexponential behavior with an average lifetime of ~2.6–2.7 ns. The reason why more fluorescence decay components can be resolved in these decays is their better statistics (e.g., the background counts are completely negligible, which is not so for the microscopic decays).

In the case of the binary equimolar mixture of DPPC and DOPC, the intensity image shows a high degree of heterogeneity, with bright and dark domains (Fig. 1, *G* and *J*). This can only be due to a preference of the probe for the fluid phase, because the quantum yield of the probe is similar for both pure phases. In the equatorial section of the GUVs (Fig. 1 *G*), punctuated domains are observed. From the polar picture (Fig. 1 *J*), it can be seen that the domains have complex percolative-like shape, which are sectioned in the equatorial view. This is in agreement with confocal microscopy studies of similar lipid mixtures; see, e.g., (15,28). The fluorescence lifetime image of the equatorial section shows yellowish and greenish regions (Fig. 1 *H*) in the lifetime color scale (Fig. 1 *I*). Even in areas that correspond to maximum intensity in the intensity image, it is possible to distinguish different colors in the FLIM. On another hand, the longer lifetime in the distribution histogram is ~2.3 ns, showing that even the bright areas in the intensity image do not correspond to a pure fluid DOPC-rich phase, i.e., the gel/fluid lipid domains have some kind of substructure that is not resolvable by fluorescence intensity images. The histogram with the pixel distribution of lifetimes is now broader and shifted to lower values as compared with the pure phases, both in the equatorial and in the polar sections (Fig. 1, *I* and *L*). This is a striking feature, once that the lifetime is the same in the gel and in the fluid phases. The microscopic decays become biexponential for the binary mixture (Table 1), with a component at ~0.6 ns, and another component of 2.6–2.7 ns similar to the one observed for the pure phases. The lifetime averaged by the normalized amplitudes has a value of ~2.2 ns, whereas the average lifetime is almost not affected

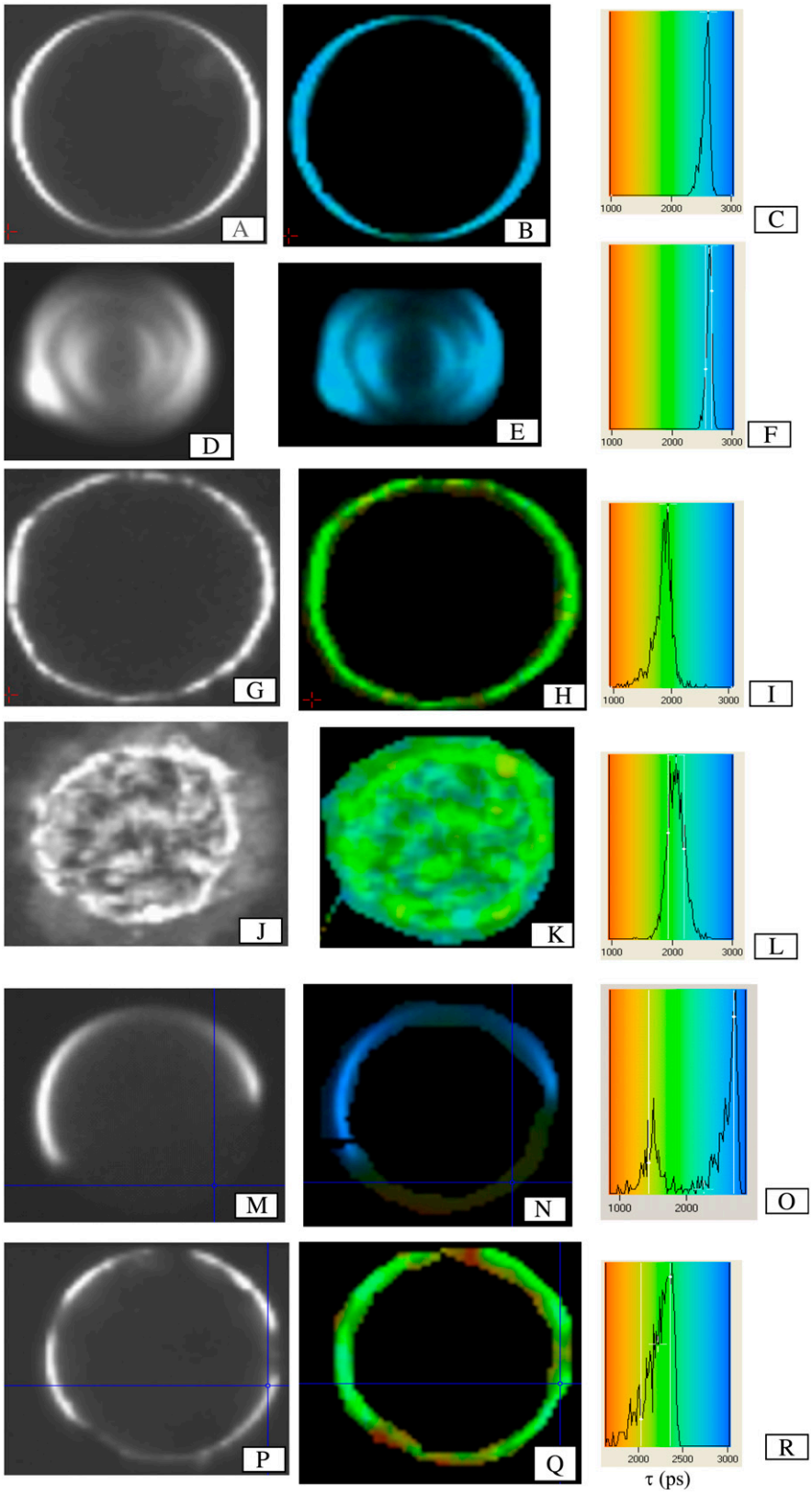


FIGURE 1 Two-photon ($\lambda_{excitation} = 860$ nm) excitation fluorescence intensity image (*left panels*), fluorescence lifetime (FLIM) image (*middle panels*), and fluorescence lifetime distribution histogram of the respective FLIM image (*right panels*) of vesicles composed of DOPC, DPPC, and cholesterol, in different mole fractions, at room temperature (24°C), labeled with Rhod-DOPE (0.2 mol %). The DOPC/DPPC/cholesterol mole ratios are 1:0:0 (*A–C*); 0:1:0 (*D–F*); 1:1:0 (*G–L*); 1:1:1 (*M–O*); and 1:1 + 12 mol % (*P–R*). The images correspond to equatorial sections of GUVs (diameter between 12 and 25 $\mu$m), except for panels *D*, *E* (section of an MLV), *J*, and *K* (*top view* of a GUV). The color code used in the FLIM images is the one indicated in the histograms on the right.

**TABLE 1 Parameters describing representative microscopic fluorescence intensity decays (Eq. 1) of Rhod-DOPE (0.2 mol %) incorporated in GUVs composed of different mole fractions of DOPC, DPPC and cholesterol, at room temperature (24°C)**

| Sample | $\alpha_1$ | $\tau_1$ | $\alpha_2$ | $\tau_2$ | $\langle\tau\rangle$ (ns) | $\bar{\tau}$ (ns) | $\chi^2$ |
|---|---|---|---|---|---|---|---|
| DOPC | 1 | 2.64 | 0 | — | 2.64 | 2.64 | 1.04 |
| DPPC | 1 | 2.60 | 0 | — | 2.60 | 2.60 | 1.39 |
| DOPC/DPPC 1:1 equator (with dark and bright areas) | 0.76 | 2.69 | 0.24 | 0.56 | 2.56 | 2.18 | 1.07 |
| DOPC/DPPC 1:1 pole (bright area) | 0.99 | 2.62 | 0.01 | 1.08 | 2.61 | 2.61 | 2.1 |
| DOPC/chol 9:1 | 0.83 | 2.80 | 0.17 | 0.53 | 2.71 | 2.42 | 1.51 |
| DOPC/chol 4:1 | 0.85 | 2.58 | 0.15 | 0.76 | 2.49 | 2.31 | 1.41 |
| DOPC/chol 7:3 | 0.89 | 2.62 | 0.11 | 0.80 | 2.55 | 2.42 | 1.61 |
| DPPC/chol 9:1 | 0,94 | 2,66 | 0,06 | 1,21 | 2.62 | 2.57 | 1.54 |
| DPPC/chol 3:1 | 0.90 | 2.50 | 0.10 | 0.53 | 2.46 | 2.31 | 1.32 |
| DPPC/chol 7:3 | 0.90 | 2.47 | 0.10 | 0.29 | 2.45 | 2.26 | 1.70 |
| DPPC/chol 3:2 | 0.87 | 2.51 | 0.13 | 0.59 | 2.44 | 2.25 | 1.26 |
| DOPC/DPPC 1:1 + 6 mol % chol homogeneous bright pole | 0.78 | 2.73 | 0.22 | 0.42 | 2.63 | 2.21 | 0.96 |
| DOPC/DPPC 1:1 + 6 mol % chol heterogenous area | 0.79 | 2.52 | 0.21 | 0.26 | 2.46 | 2.05 | 1.00 |
| DOPC/DPPC 1:1 + 9 mol % chol homogeneous pole | 0.82 | 2.53 | 0.18 | 0.672 | 2.43 | 2.20 | 1.14 |
| DOPC/DPPC 1:1 + 9 mol % chol dark domain | 0.83 | 2.07 | 0.17 | 0.35 | 2.01 | 1.77 | 1.22 |
| DOPC/DPPC 1:1 + 12 mol % chol bright domain in the equator | 0.93 | 2.68 | 0.07 | 0.44 | 2.66 | 2.52 | 1.36 |
| DOPC/DPPC 1:1 + 12 mol % chol previous GUV, dark domain near pole | 1 | 1.91 | 0 | — | 1.91 | 1.91 | 1.09 |
| DOPC/DPPC 1:1 + 12 mol % chol another dark domain | 1 | 1.88 | 0 | — | 1.88 | 1.88 | 1.15 |
| DOPC/DPPC 1:1 + 12 mol % chol homogeneous pole | 0.81 | 2.49 | 0.19 | 0.361 | 2.43 | 2.10 | 1.14 |
| DOPC/DPPC 1:1 + 33 mol % chol centered in a raft near equator | 0.74 | 2.83 | 0.26 | 0.49 | 2.70 | 2.22 | 0.96 |
| DOPC/DPPC 3:7 heterogeneous area | 0.70 | 2.54 | 0.30 | 0.66 | 2.36 | 1.98 | 1.58 |
| DOPC/DPPC 3:7 bright domain | 1 | 2.56 | 0 | — | 2.56 | 2.56 | 1.61 |
| DOPC/DPPC 3:7 + 9 mol % chol bright region on equator | 0.69 | 2.17 | 0.31 | 0.44 | 2.02 | 1.63 | 1.32 |
| DOPC/DPPC 3:7 + 9 mol % chol bright pole | 0.87 | 2.59 | 0.13 | 0.74 | 2.51 | 2.35 | 1.58 |
| DOPC/DPPC 3:7 + 9 mol % chol | 1 | 2.12 | 0 | — | 2.12 | 2.12 | 1.57 |

The decays were obtained under the two-photon microscope ($\lambda_{excitation} = 860$ nm), with the laser fixed in a specific region of a GUV. When different decays were obtained in different regions of GUVs with the same composition (or in a single GUV), the details of laser location are discriminated. The average lifetime (Eq. 2) and the lifetime-weighted quantum yield (Eq. 3) are also given. Chol stands for cholesterol.

(~2.5–2.6 ns). The macroscopic decay in MLV suspension shows similar features (Table 2). The shorter component in the macroscopic decays is longer than in the microscopic ones. This is not surprising, because a very specific region of a GUV is probed in the latter one, which is not expected to reflect the ensemble average value of the former.

Similar results were obtained for the mixtures DOPC/DPPC (3:7 mol/mol). The microscopic decays for these mixtures are given in Table 1.

## DOPC/cholesterol and DPPC/cholesterol binary mixtures

In the case of DOPC/cholesterol mixtures, there is a slight decrease of the lifetime upon increasing cholesterol mole fraction in GUVs, as shown in the lifetime histograms of Fig. 2 *A* (*solid lines*). There is no observation of domains in the intensity image, neither on the FLIM image (not shown). The microscopic decays do not show any clear trend with

**TABLE 2 Parameters describing representative macroscopic (ensemble) fluorescence intensity decays of Rhod-DOPE (0.2 mol %) incorporated in MLVs (or LUVs where indicated) composed of different mole fractions of DOPC, DPPC, and cholesterol, at room temperature (24°C); $\lambda_{excitation} = 575$ nm**

| Sample | $\alpha_1$ | $\tau_1$ | $\alpha_2$ | $\tau_2$ | $\langle\tau\rangle$ (ns) | $\bar{\tau}$ (ns) | $\chi^2$ |
|---|---|---|---|---|---|---|---|
| DOPC (LUV) | 0.82 | 2.98 | 0.18 | 1.63 | 2.66 | 2.58 | 1.07 |
| DPPC | 0.96 | 2.66 | 0.04 | 1.27 | 2.64 | 2.61 | 1.24 |
| DOPC/DPPC 1:1 (LUV) | 0.74 | 2.51 | 0.26 | 1.25 | 2.32 | 2.17 | 1.11 |
| DOPC/chol 3:1 | 0.77 | 2.72 | 0.23 | 1.66 | 2.55 | 2.48 | 1.16 |
| DOPC/chol 3:2 | 0.79 | 2.60 | 0.21 | 1.37 | 2.46 | 2.35 | 1.12 |
| DPPC/chol 3:1 | 0.33 | 2.32 | 0.67 | 1.40 | 2.11 | 2.02 | 1.15 |
| DPPC/chol 3:2 | 0.31 | 2.69 | 0.69 | 1.45 | 1.99 | 1.82 | 1.06 |
| DOPC/DPPC 1:1 + 10 mol % cholesterol | 0.74 | 2.65 | 0.26 | 1.52 | 2.46 | 2.36 | 1.17 |
| DOPC/DPPC 1:1 + 33 mol % cholesterol | 0.66 | 2.55 | 0.34 | 1.53 | 2.31 | 2.20 | 1.09 |
| DOPC/DPPC 1:1 + 50 mol % cholesterol | 0.63 | 2.37 | 0.37 | 1.35 | 2.11 | 1.99 | 1.07 |

The average lifetime (Eq. 2) and the lifetime-weighted quantum yield (Eq. 3) are also given.

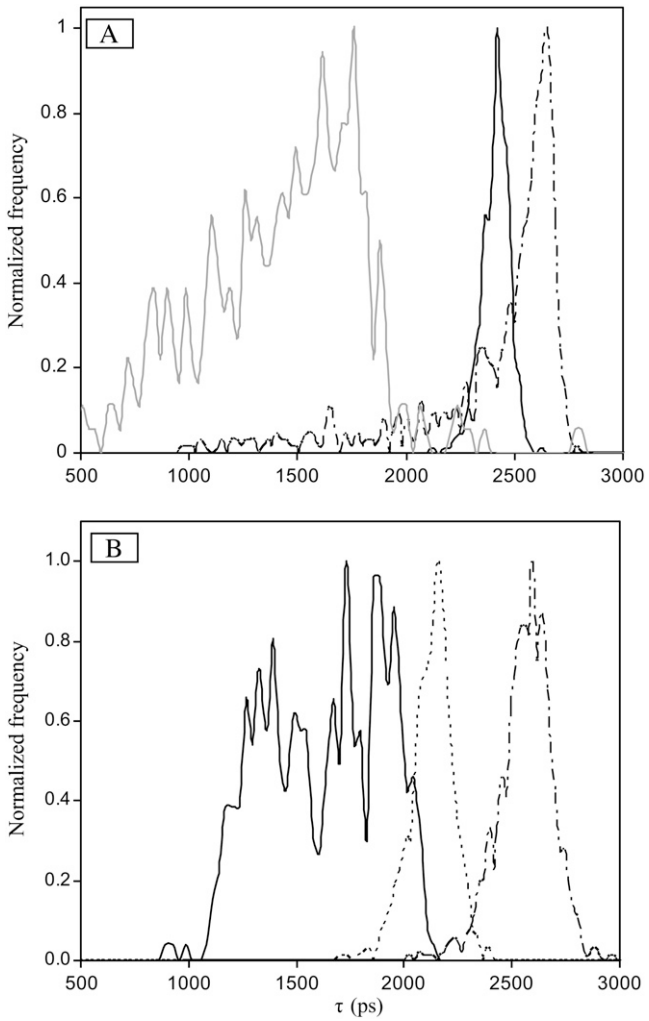


FIGURE 2 Representative fluorescence lifetime distribution histograms corresponding to FLIM images of GUVs labeled with Rhod-DOPE (0.2 mol %), at room temperature (24°C), composed of (*A*) DOPC (*dashed line*), DOPC/cholesterol 7:3 (*solid line*), and DOPC/DPPC/cholesterol 1:1:2 (*shaded line*); and (*B*) DPPC/cholesterol 1:0 (*dashed-dotted line*), 4:1 (*dotted line*), and 7:3 (*solid line*).

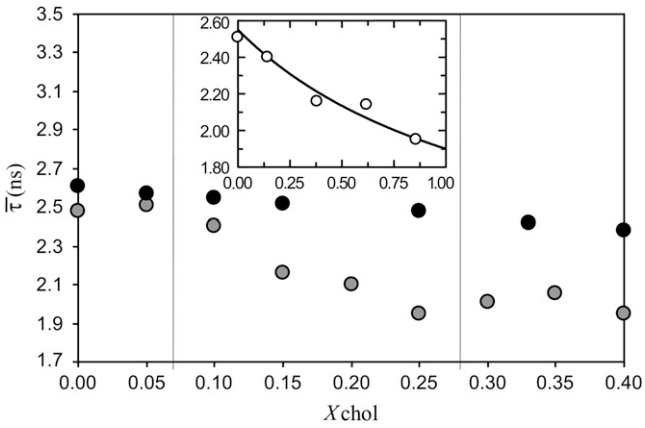


FIGURE 3 Lifetime-weighted quantum yield of Rhod-DOPE (calculated from the macroscopic fluorescence intensity decays, Eq. 3) incorporated in MLVs composed of DOPC/cholesterol (*solid dots*) and DPPC/cholesterol (*shaded dots*) as a function of cholesterol content, at room temperature (24°C). The dotted lines indicate the $l_d/l_o$ phase coexistence boundaries taken from the DPPC/cholesterol phase diagram at that temperature (24,41,42). The inset shows the lifetime-weighted quantum yield of Rhod-DOPE incorporated in DPPC/cholesterol vesicles spanning the $l_d/l_o$ phase coexistence range, as a function of $l_o$ phase mole fraction and the fit of Eq. 5 to the data with $K_p^{(lo/gel)} = 1.9 \pm 0.5$.

cholesterol concentration (Table 1). The macroscopic fluorescence decays, however, show a clear trend with a monotonic decreasing behavior of the lifetime-weighted quantum yield of the probe, for increasing fractions of the sterol (Table 2, Fig. 3). The macroscopic measurements have the best quality, and small variations can be clearly detected (from 2.7 ns to 2.5 ns average lifetime or from 2.6 ns to 2.4 ns for the lifetime-weighted quantum yield). Such differences are not so easily resolved with the microscopic measurements.

The binary system DPPC/cholesterol showed a completely different behavior, both in GUV microscopy experiments and in MLV ensemble macroscopic decays. The fluorescence intensity and lifetime images do not show the presence of any kind of domains (not shown). Nevertheless, the lifetime distribution does change, displaying a clear decrease of the center of the distribution as seen in the histograms taken from FLIM images (Fig. 2 *B*). In addition, the microscopic decays show an increasing contribution of the short component with increasing cholesterol fraction (Table 1). The fluorescence decays in MLV suspension show a significant change (Table 2), reflected in a clear trend of the lifetime-weighted quantum yield (Fig. 3). A strong decrease is observed, similarly to what was noticed in the raft system PSM/POPC/cholesterol (9) for the same probe along a $l_d/l_o$ tie-line, and for the binary system 1,2-dimyristoyl-*sn*-glycero-3-phosphocholine (DMPC)/cholesterol above the transition temperature of DMPC, along the $l_d/l_o$ tie-lines at 30°C and 40°C with a probe analogous to Rhod-DOPE, but with myristoyl acyl chains (40). From the data in Fig. 3, and comparing it with reported gel/$l_o$ coexistence limits at room temperature (24°C) (41,42), the changes in slope of the lifetime-weighted quantum yield coincide with phase regime changes. The marked differences observed for the fluorescence lifetime microscopic parameters of the probe in the two binary systems point to a fundamental dissimilarity of behavior between them. This is certainly related to the inability of DOPC to form an $l_o$ phase in the presence of cholesterol at room temperature in opposition to DPPC (43). It is worth mentioning that the broad distribution of lifetimes retrieved from the FLIM image of DPPC/cholesterol 7:3 (Fig. 2 *B*) is also due to the low fluorescence intensity of the probe in these vesicles, which is a consequence of the reduced quantum yield of the probe in the $l_o$ phase. The number of counts per pixel is lower, the statistics becomes poorer, the uncertainty in the retrieved lifetime values is higher, and the distribution becomes broader, even though a single phase is present.

It was noticed previously that Rhodamine-type probes have different photophysical behavior in $l_o$ phases, as compared to gel or $l_d$ phases; moreover, it was verified that the fluorescence lifetime of octadecyl-Rhodamine B was highly reduced upon increasing probe concentration in egg PC/cholesterol (1:1) vesicles, whereas in egg PC vesicles the fluorescence lifetime of the probe underwent only a very small decrease (44). To confirm that the different behavior observed in DPPC/cholesterol and DOPC/cholesterol (Tables 1 and 2, Figs. 2 and 3) is indeed a consequence of $l_o$ phase formation, a concentration dependence study of Rhod-DOPE fluorescence lifetime was performed in MLVs of DPPC/cholesterol (3:2), DOPC/cholesterol (3:2), and pure DOPC, i.e., $l_o$ phase, $l_d$ phase rich in cholesterol, and $l_d$ phase without cholesterol, respectively. The latter one was to confirm that the presence of cholesterol per se is not sufficient to strongly reduce the fluorescence lifetime of Rhod-DOPE. The results are displayed in Fig. 4, where the average lifetime of Rhod-DOPE is represented as a function of probe concentration (*left panel*). It can be clearly observed that 1), the average fluorescence lifetime of Rhod-DOPE tends to reach the same value for infinite dilution of the probe in all systems studied; 2), in the case of $l_d$ phases, both with and without cholesterol, the variation of the lifetime with probe concentration is small (although in the case of DOPC/cholesterol, the decrease is more noticeable, which will be justified later on); and 3), in the case of the $l_o$ phase, a strong decrease occurs to a value much lower than any value observed for the other two systems in the concentration range studied, with an (apparently) hyperbolic behavior. This result demonstrates once again a fundamental difference between the DPPC/cholesterol (3:2) system, and the other two systems, related to the formation of the $l_o$ phase. In addition, in the inset a Stern-Volmer plot for the DPPC/cholesterol system is given. A dynamic self-quenching process in a time-resolved fluorescence experiment is described by the Stern-Volmer equation

$$\bar{\tau}_0/\bar{\tau} = 1 + k_q\langle\tau\rangle_0[\mathrm{F}], \tag{4}$$

where $\langle\tau\rangle$ and $\bar{\tau}$ have the usual meanings (Eqs. 2 and 3, respectively), the subscript *0* indicates infinite dilution the product $k_q\langle\tau\rangle_0$ is the Stern-Volmer constant, and [F] is the fluorophore concentration. Accordingly, if the dynamic quenching process is the main mechanism responsible for the fluorescence lifetime decrease of the probe upon increasing its concentration, then a plot of $\bar{\tau}_0/\bar{\tau}$ as a function of Rhod-DOPE concentration should be linear with intercept 1. This is, in fact, the result depicted in the inset of Fig. 4.

The lifetime-weighted quantum yield variation as a function of membrane composition within a phase coexistence range (i.e., along a tie-line) can be used to calculate a partition coefficient of the fluorescent probe between the two coexisting phases 1 and 2, $K_p$. This is achieved by fitting the equation

$$\bar{\tau} = (\bar{\tau}_1 K_p X_1 + \bar{\tau}_2 X_2)/(\bar{\tau}_1 X_1 + \bar{\tau}_2 X_2), \tag{5}$$

to the experimental data (e.g., (9)). In this expression, $\bar{\tau}_i$ and $X_i$ are the amplitude-averaged lifetime of probe in phase $i$ (Eq. 3), and mole fraction of that phase, respectively. The phase mole fractions are calculated by applying the lever rule. Using the data in Fig. 3, for the DPPC/cholesterol mixture between the two-phase boundaries, a $K_p^{(lo/gel)} = 1.9 \pm 0.5$ is obtained. The probe shows a slight preference for the phase $l_o$. However, this preference is not as marked as the preference for the $l_d$ phase in relation to the $l_o$, for which a $K_p^{(ld/lo)} = 2.9 \pm 0.6$ is reported (9,45). By combining these two values, it is possible to estimate a value for $K_p^{(ld/gel)} \approx K_p^{(ld/lo)} \times K_p^{(lo/gel)} = 5 \pm 2$ (overcoming the limitation originated by the similarity of the fluorescence lifetime of Rhod-DOPE in pure $l_d$ and pure gel phases). This value demonstrates a strong preference of the probe for the fluid phase, as expected, because of its unsaturated acyl chains and bulky headgroup.

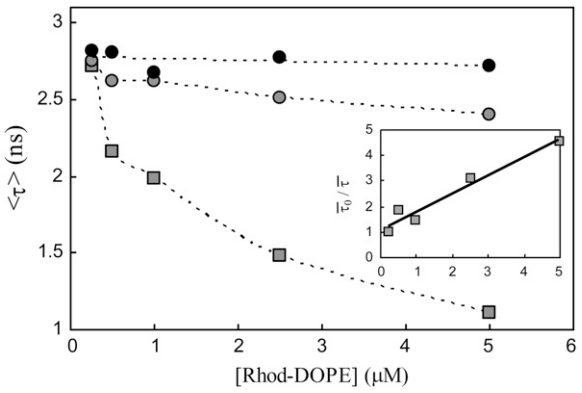


FIGURE 4 Average fluorescence lifetime of Rhod-DOPE (calculated from the macroscopic fluorescence intensity decays, Eq. 2) as a function of probe concentration incorporated in MLVs of DOPC (*solid circles*), DOPC/cholesterol 3:2 (*shaded circles*), and DPPC/cholesterol 3:2 (*shaded squares*), at room temperature (24°C). The lines are merely guides to the eye. (*Inset*) Stern-Volmer plot (Eq. 4) for Rhod-DOPE in DPPC/cholesterol 3:2 MLVs at 24°C.

## DOPC/DPPC/cholesterol ternary mixtures

The region corresponding to DOPC/DPPC 1:1 mol/mol with different cholesterol concentrations was also explored. By fixing the proportion of two components and varying the fraction of a third one, different regions of a phase diagram with different number and types of phases are covered.

For 50 mol % cholesterol (DOPC/DPPC/cholesterol 1:1:2) a completely homogenous fluorescence lifetime pattern is observed (not shown), corresponding to a broad distribution with maximum at ~1.6–1.8 ns (Fig. 2 *A*). The total intensity (average count rate) is clearly lower than in vesicles without cholesterol, as also observed in epifluorescence mode of the FLIM system using a mercury lamp as the light source

(results not shown). The fluorescence lifetime histogram plot is more noisy than for a pure fluid or a pure gel phase (compare with the histograms for DOPC and for DPPC in Fig. 2). This clearly indicates that the vesicles are completely in $l_o$ state for the mixture 1:1:2, in which the probe has a lower quantum yield (and so a shorter fluorescence lifetime). Note that the noise broadens the fluorescence lifetime distribution, but would never give rise to values longer than 0.5 ns. Pixels with very low photon counts present fluorescence decays close to the background decays and the program either recognizes this pixel as one without intensity, or attributes it to a very short lifetime, usually of $<$100 ps. In the present work, fluorescence lifetime values $<$0.3 ns in a FLIM image were not considered as statistically meaningful. However, for the high count microscopic decays (fixed laser beam configuration) and for the macroscopic decays, short components of $<$300 ps can be detected and are statistically significant. The macroscopic decay is again complex (Table 2), but the lifetime averaged by the amplitudes is in very good agreement with the lifetime histogram.

For the DOPC/DPPC/cholesterol 1:1:1 composition, a clear $l_d/l_o$ phase coexistence is present (Fig. 1, *M* and *N*). Interestingly, in the 1:1:1 mixture, the dark domains coalesced into one big dark domain, as observed by others (27) whereas for other compositions, a complex pattern persisted throughout the experiment (see below). This is illustrated in Fig. 1 *M*, where the intensity image of the equatorial section of a GUV with equimolar composition is shown. To the bright and dark domain correspond a specific color in the FLIM image (Fig. 1 *N*), and the pixel lifetime histogram is bimodal, with two sharp peaks—one centered at ~1.7 ns, and the other centered at ~2.8 ns (Fig. 1 *O*). These peaks correspond to the brown (*dark*) domain, i.e., the raft ($l_o$) phase, and to the blue (*bright*) domain, i.e., the nonraft ($l_d$) phase, respectively.

For 3 and 6 mol % cholesterol, the pattern is similar to the one observed for the 1:1 DOPC/DPPC mixture, without cholesterol (results not shown). The domain interfaces are smoother than with 0% cholesterol, but all other features are identical (e.g., the microscopic decays in Table 1). However, for 9 and 12 mol % cholesterol a more complex behavior was observed. In Fig. 1, *P–R*, the fluorescence intensity and lifetime image, and the lifetime histogram are shown for the equatorial section of a DOPC/DPPC (1:1) GUV with 12 mol % cholesterol (for 9 mol % cholesterol, the results were similar; not shown). Both the images and the histogram resemble that of the DOPC/DPPC 1:1 (0% cholesterol) vesicle (Fig. 1, *G–I*). However, in the 12 mol % cholesterol GUVs, the domains are less punctuated, and the lifetime histogram shows higher frequency values close to the maximum 2.5 ns lifetime, with a consequent suggestion of three types of domains: bluish ($\tau$ ~2.5 ns); greenish ($\tau$ ~2.2 ns), and orangish ($\tau$ ~1.9 ns). The same vesicle was imaged from the top (Fig. 5). In this case, the vesicle shows the existence of complexly shaped domains, with some black round-shaped areas. In the intensity image (Fig. 5 *A*), three regions with different levels of intensity (*shaded*, *open*, and *solid*) are apparent, although it is difficult to establish an objective criterion in such a type of image. However, in the lifetime image (Fig. 5 *B*) there are clearly light-to-dark-blue domains ($\tau$ ~2.3–2.5 ns, and black round domains surrounded by a red halo ($\tau$ < 1.3 ns). In between them, a green-yellow ($\tau$ ~1.4–2.0 ns) area with percolative-like structure is present. The black color in the FLIM image indicates that along all the time channels the count number is similar or inferior to the background level. The distinction between three regions in the top view of the vesicle is perfectly clear in the fluorescence lifetime image; see phase assignment in the intensity image (Fig. 5 *A*). The histogram (Fig. 5 *C*) is broader than for the DOPC/DPPC mixture (0% cholesterol; Fig. 1, *I* and *L*), particularly in the low lifetime range.

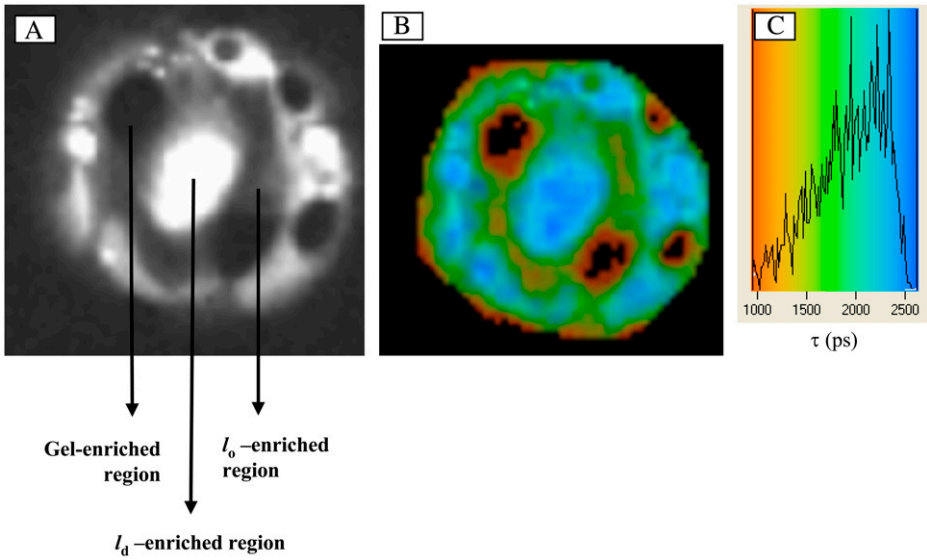


FIGURE 5 Two-photon ($\lambda_{excitation}$ = 860 nm) excitation top view fluorescence intensity image (*A*), fluorescence lifetime (FLIM) image (*B*), and fluorescence lifetime distribution histogram of the respective FLIM image (*C*) of a 24-$\mu$m diameter GUV composed of DOPC, DPPC in a 1:1 mol ratio with 12 mol % cholesterol, labeled with Rhod-DOPE (0.2 mol %), at room temperature (24°C). The color code used in the FLIM image is the one indicated in the histogram. Solid spots inside the vesicle correspond to pixels with counts equal or below the background level. The equatorial section of the same vesicle is shown in Fig. 1, panels *P–R*. In the intensity image (*A*), examples of regions that can be safely assigned to a certain phase behavior based on the fluorescence lifetime of Rhod-DOPE (*B*) are indicated.

Four high-count microscopic decays were obtained in one GUV with the composition DOPC/DPPC (1:1) + 12 mol % cholesterol (Table 1). The first decay obtained, in a bright region of the vesicle, is almost monoexponential, pointing to a particularly fluid-enriched area. The other two decays were obtained with the laser pointing to a domain with a similar aspect to the dark domain on the right side of the equator shown in Fig. 1 *P*. In this case, a monoexponential decay with a lifetime of 1.9 ns was retrieved, indicative of a raftlike ($l_o$) domain. Finally, a biexponential decay typical of gel/fluid coexistence, as in the absence of cholesterol, was obtained in another region of the same vesicle.

Similar results and conclusions were obtained for the mixtures DOPC/DPPC (3:7 mol/mol) with 9 mol % of cholesterol. The microscopic decay parameters for these mixtures are given in Table 1.

## DISCUSSION

### Microscopic and macroscopic decays in pure lipid phases

The emission decay of Rhod-DOPE in the pure gel and in the pure fluid phases presents very similar fluorescence lifetimes. Though the macroscopic decays show a more complex profile even in the pure lipid phases, the lifetime weighted quantum yield, which is the one to compare for a first general picture, is in full agreement with the microscopic decays. The macroscopic decay is, in fact, monoexponential for the lower probe concentrations in all the systems studied in Fig. 4 (data not shown).

The lifetime obtained in different experiments for a fluid $l_d$ phase (considering both the pure and the coexisting $l_d$) can range up to ~3 ns, which is similar to the value obtained in the ternary raft mixture PSM/POPC/cholesterol (9) with composition corresponding to a pure fluid ($l_d$) phase.

Overall, considering all the instrumental, and sample differences, the agreement between the macroscopic and microscopic decays in the pure phases is very good (it is within ± 0.1 ns).

However, the small differences verified among the lifetime values in MLV and LUV suspension and under the TPE microscope both for GUVs and MLVs and the difference in the number of components in the fluorescence decay should be discussed. The excitation process (one-photon versus two-photon) does not influence the excited state lifetime, but if there are multiple emitting species (e.g., monomers, dimers) with different absorption bands, and different fluorescence lifetimes, some differences can arise. In addition, the TPE cross-section is different from the one-photon absorption spectrum of the probe. This would lead to more significant differences than those observed: namely, the excellent agreement of the lifetime-weighted quantum yield obtained from the different methodologies used in the present work would not occur. Additionally, the vesicle type is not important, because Rhod-DOPE shows the same fluorescence intensity decay behavior between MLVs and LUVs in the macroscopic decay (Table 2), and also between MLVs and GUVs in the microscopic decays (image, Fig. 1, *E* and *F*; and microscopic, Table 1). Another possibility is that a slightly different concentration of probe occurs, due to incomplete lipid hydration in GUVs. As shown in Fig. 4 and in MacDonald (44), the photophysics of Rhodamine-probes is concentration-dependent in a manner characteristic of the lipid system where it is incorporated. However, a quantitative concentration dependence study in GUVs is hampered by the fact that the experimental range of probe concentrations accessible is not very large, due to the indispensable compromise between a reasonable number of counts per pixel required to have good fluorescence decay statistics, and a sufficiently low concentration to approach the infinite dilution regime.

### Gel-fluid phase coexistence

In the GUVs with gel-fluid coexistence, most of the high count microscopic decays had to be analyzed using a biexponential model, retrieving a short component with a lifetime different from any component observed in the macroscopic decay for the pure phases. The long component of the microscopic decay is still reflecting the average macroscopic lifetime of the probe in the pure phases. The biexponential behavior of the microscopic decay observed in the gel/fluid mixtures can thus be used as a fingerprint for gel/fluid coexistence (Table 1). It is important to note that a monoexponential behavior can also be obtained for this lipid mixture, depending on the region of the GUV under observation. Therefore, to perform a complete characterization of the lipid phase coexistence, high count microscopic decays from different regions of the same GUV may be needed. Some of these decays can be different from the macroscopic decay, because this one is an average of all the lipid phases and interfaces present in the system. The origin of the short component is not completely clear, and it is not the goal of the present work to determine it, but it is probably due to accumulation of probe in the interfaces of the gel/fluid domains, where a much higher local probe concentration would occur. This would lead to a more efficient self-quenching, and could also favor dimer formation (leading namely to monomer-dimer FRET). Both processes are known to reduce the Rhodamine-type probes fluorescence lifetime (44). The interface between the domains could thus favor the formation of Rhodamine aggregates due to a very high local probe concentration, on one hand, and the head group labeling favors the appropriate stacking of the xanthene rings of the fluorophore, on the other. The structure of Rhodamine dimers was previously described as a face-to-face stacking of the xanthene rings with sub-nanosecond fluorescence lifetime (46), similar to the short component detected in the present work for the gel/fluid GUVs. The fact that in the

microscopic decays the fraction attributed to the short component is always small also supports the interface location interpretation of its origin, because the interfacial lipid fraction is always small compared to the bulk lipid fraction.

## Phospholipid/cholesterol binary mixtures

In the case of DOPC/cholesterol mixtures, the mean fluorescence lifetime changes from 2.6 ns to 2.3 ns (Figs. 2 *A* and 3, and Tables), with increasing cholesterol mole fraction, at a fixed probe/lipid ratio. The macroscopic decays have the best quality among the different types of fluorescence decays obtained in this study, and in this way, they are sensitive even to small variations. The variation observed for the DOPC/cholesterol system is a small and continuous one that is reporting no phase transition. It is solely due to the replacement of DOPC by cholesterol that leads to a lipid bilayer with lower mean surface molecular area, resulting in a higher local probe concentration, and thus a shorter fluorescence lifetime.

In the case of DPPC, however, the formation of $l_o$ in DPPC/cholesterol is clear from the steep decrease in the lifetime-weighted quantum yield, and the complex trend of variation with cholesterol mole fraction is indicative of phase separation. However, this phase separation leads to the formation of lipid domains with size below resolution of TPE (this work) and one-photon excitation (19) fluorescence microscopy.

The variation of lifetime-weighted quantum yield between the gel/$l_o$ phase coexistence boundaries is well described by Eq. 5, which assumes ideal partition of the fluorescent probe between two lipid phases. The partition coefficient obtained indicates a preference of Rhod-DOPE for the phase $l_o$. It is not a very strong preference, as expected, because the probe has unsaturated acyl chains that are difficult to accommodate in those phases where all-*trans* conformations prevail.

It is interesting to discuss why there is a strong decrease of the fluorescence lifetime of Rhodamine when changing from an $l_d$ or a gel phase to a $l_o$ phase. The mean lipid molecular surface area is approximately as small in the gel, as in $l_o$ phases. Thus, the probe surface density is high in both of them (compared to the $l_d$). The surface area of cholesterol is lower than that of a PC molecule either in the gel or in the fluid phase, and when $l_o$ formation occurs, a well-known condensing effect happens, further reducing the mean molecular area (e.g., (9)) which is therefore even smaller than the one in the gel. However, the $l_o$ phase retains a high degree of translational mobility, with a lateral diffusion coefficient no more than one order-of-magnitude smaller than in the $l_d$ phase (e.g., (11,16)), but still several orders-of-magnitude above that of the gel phase. The dynamic quenching processes are still effective in $l_o$, whereas in the gel phase they should not lead to a significant degree of quenching, because the lateral diffusion coefficient is quite low. On another hand, by increasing the probe's surface density relatively to the $l_d$, dimer formation is also favored. In this way, the phase $l_o$ maximizes the processes that lead to a decrease of Rhodamine-probes fluorescence lifetime. The fact that in DOPC/cholesterol 3:2 the average fluorescence lifetime of Rhod-DOPE decreases more with probe concentration than in pure DOPC (with a mean molecular area 30% larger than that of the cholesterol-containing vesicles), but is still much higher than in DPPC/cholesterol vesicles (Fig. 4), further supports the interpretation given above.

## DOPC/DPPC/cholesterol ternary mixtures

The results obtained for compositions in well-defined regions of the phase diagram can be easily interpreted, and this knowledge can then be applied to more obscure regions to gain new insights on the system behavior in those regions. This was the goal of the present work. The DOPC/DPPC/cholesterol system has been studied by other techniques, and is well characterized (27,28).

The fluorescence lifetime of a probe can be altered, even when the lipid phase remains the same, in case some property of the system undergoes a change (e.g., of composition or temperature). Most important for Rhod-DOPE, is the fact that the composition is directly related to the mean molecular area and thus to the probe's surface density (concentration), leading to fluorescence lifetime variations, as a result of the dynamic self-quenching interaction (Fig. 4). Changes in lifetime can also be due to experimental difficulties; for example, keeping the same probe concentration either in every observed GUV, or from sample to sample. In this way, it is important to establish the boundaries for the parameter that are typical of a certain phase. The criteria for phase assignment are given in Table 3. The $l_d/l_o$ phase coexistence is clearly different from the gel/fluid coexistence. In general, it is well known that the shape of the domains is quite different, being more round in the fluid/fluid case, and much more complex in the gel/fluid situation. The fluorescence lifetime of Rhod-DOPE in $l_d$ and $l_o$ is clearly different, and for compositions with significant fraction of both phases it is possible to obtain bimodal histograms of the FLIM image lifetime distributions (Fig. 1 *O*).

For the typical probe concentrations, the lifetime-weighted quantum yield of the probe is approximately half in the $l_o$ phase coexisting with the $l_d$ in the 1:1:1 mixture (Table 3), as already verified previously by bulk fluorescence spectroscopy for the PSM/POPC/cholesterol system along the $l_o/l_d$ tie-line containing the 1:1:1 composition (9), and along two $l_o/l_d$ tie-lines of the DMPC/cholesterol system (40). Several conclusions can be drawn from these results taken altogether:

1. The tie-line used in the cited FRET study determined by a bulk spectroscopic approach (8) for a similar raft system (POPC/PSM/cholesterol) is in agreement with the results of the present work, and points to a general

**TABLE 3 General behavior of the macroscopic and microscopic time-resolved fluorescence of Rhod-DOPE in the ternary lipid system DOPC/DPPC/cholesterol at 24°C in different situations of one-phase or two-phase coexistence**

| Phase (or phase coexistence) | Intensity image | Individual microvolume decay | Lifetime image distribution histogram | Macroscopic decay |
|---|---|---|---|---|
| Pure gel or fluid | Homogeneous. | Monoexponential, 2.6–2.8 ns. | Sharp, centered at 2.6–2.7 ns. | Biexponential, $\bar{\tau}\sim$ 2.6–2.8 ns. |
| Pure $l_o$ | Homogeneous, low intensity. | Biexponential, $\bar{\tau}\sim$ 1.8–2.2 ns. | Noisy, centered at ~1.6 ns. | 1.6–2.0 ns. |
| Gel/$l_d$ | Highly heterogeneous with percolative domains. | Similar to pure gel or fluid phase, or biexponential,* $\bar{\tau}\sim$ 2.0–2.2 ns.† | Broad approximate symmetric distribution between ~1.6 and 2.5 ns. | Biexponential, $\bar{\tau}\sim$ 2.2 ns.† |
| Gel/$l_o$ | Homogeneous, intensity decreasing with $l_o$ fraction. | Biexponential, depends on phase fraction. | Sharp to slightly broadened. | Biexponential, depends on phase fraction. |
| $l_d/l_o$ | Round coalescing bright ($l_d$) and dark domains ($l_o$). | Biexponential, depends on phase fraction. | Bimodal with one peak at typical $l_o$ value and another at typical $l_d$ value. | Biexponential, depends on phase fraction. |

The values indicated correspond to typical concentrations of probe used in this type of studies (~0.1–0.5 mol %).
*Depending on the region of the GUV.
†For the compositions covered in this study DOPC/DPPC (1:1) and (3:7).

behavior of the fluorescence lifetime of Rhodamine-head labeled membrane probes that can be applied to the detection of cholesterol-enriched domains in more complex systems, such as reconstituted vesicles with purified lipids from biological sources, and even in cellular membranes.

2. The $l_d/l_o$ phase coexistence can be easily distinguished from gel/fluid, because this one leads to a different type of FLIM distribution, namely a broad histogram centered at ~2.1 ns, corresponding to a biexponential fluorescence decay with one subnanosecond component, and another component close to the one of the pure gel or fluid phases that can be detected in the microscopic decay (Table 3).

## Unraveling heterogeneity I: evidence for three-phase coexistence

By means of the careful characterization of the time-resolved microspectroscopic behavior of Rhod-DOPE in the pure DOPC (pure fluid), pure DPPC (pure gel), DOPC/DPPC/cholesterol 1:1:2 (pure $l_o$), DOPC/DPPC 1:1 (clear gel/fluid phase separation), and DOPC/DPPC/cholesterol 1:1:1 (clear $l_d/l_o$ phase separation), criteria for the coexistence of these phases could be established (Table 3), which are now used to interpret the complex results obtained for the DOPC/DPPC mixtures with lower amounts (9 and 12 mol %) of cholesterol. The intensity images for pure DOPC, pure DPPC, and DOPC/DPPC (1:1) (and also DOPC/DPPC/cholesterol 0.4/0.4/0.2, in a clear $l_d/l_o$ situation, which is identical to the 1:1:1 image presented here—Fig. 1 *M*) obtained with a cyanine dye ($DiIC_{18}$) for a probe/lipid ratio of 1:1000 in a confocal microscope (one-photon excitation) (28) are similar to the intensity images obtained in the present work, showing that the general behavior of the system and domains observed are independent of the excitation method, type of probe and probe/lipid ratio (see Materials and Methods). In this way, the combination of the information obtained from the intensity images with that from the lifetime pictures, to further detail the description of the lipid phases, is undoubtedly allowed.

In the vesicle of Fig. 5, it is clear that three phases coexist. A fluorescence lifetime $\tau$ ~2.3–2.5 ns in bright areas indicates that this is a fluid ($l_d$) enriched area. However, it presents a lifetime shorter than the typical values for pure $l_d$ phase, though it corresponds apparently to one-phase areas (Fig. 5 and Table 1). The remaining components correspond to $l_o$ (lower lifetime, lower intensity), and the interface is very extensive and ramified. There are dark round domains surrounded by areas with the 1.5–1.8 ns typical of $l_o$. These domains are black because the number of counts is at the background level. In the presence of three phases, the probe has to be distributed among them according to the partition coefficient values. Thus, due to a $K_p^{ld/gel}$ of 5, and a similar quantum yield in both phases, in the fluid-enriched regions the average intensity should be approximately five-times greater than that in gel enriched areas. In the case of gel/$l_o$ domains, the fluorescence intensity ratio gel/$l_o$ is given by

$$I_F^{gel}/I_F^{lo} = K_p^{gel/lo}\,\bar{\tau}_{gel}/\bar{\tau}_{lo}, \quad (6)$$

which is ~0.75 considering the total probe: lipid ratio used, or even lower for smaller probe concentrations, where the lifetime ratio becomes closer to one and the ratio becomes closer to $K_p^{gel/lo} = (K_p^{lo/gel})^{-1} = 0.53$ (Fig. 3). Actually, the true ratio should lie between these two values, because the concentration of probe in both $l_o$ and gel is smaller than the total concentration because the $l_d$ phase is probe-enriched relatively to any of the other two phases. This means that the domains with lower intensity correspond to gel domains. These domains are preferentially surrounded by $l_o$-enriched areas that comprise most of the interface to the fluid-enriched domains. In this three-phase situation, the shape of the gel and $l_o$ domains is different from that of the coexistence of each of these phases with the $l_o$ phase. The progressive change in hydrophobic thickness from gel-to-$l_o$-to-$l_d$, results in the performance of the phase with intermediate properties ($l_o$) as a wetting layer stabilizing the interface between the

gel and the fluid. In this way, the gel (and $l_d$) domains become approximately round, and their size is limited as well. It is smaller than the size of $l_d/l_o$ domains in the 1:1:1 mixture, for example (Fig. 1 *M*).

The domains in this system are quite immobile, and this explains how it is possible to obtain a lifetime image (which requires much longer acquisition times than a fluorescence confocal image) and there are round-shaped areas that have a number of counts equivalent to the background level, i.e., this is a strong proof that there is no intermixing of fluorescence from different lipid domains. The immobility of the domains is probably also a consequence of the stabilization of the complex percolative structure of the domains through the presence of three phases with biophysical properties that change more progressively from one to the other than when only two of these phases are present.

In addition, the high count number microscopic decays are in agreement with this description (Table 1). It is worth noting that with an ensemble measurement it would be impossible to simultaneously discriminate the presence of three phases. In fact, the decay in a ''pure raft'' $l_o$ phase was obtained in a complex mixture such as that of Fig. 5, revealing that the interface between the gel-enriched and the fluid-enriched domains is (almost) completely constituted by $l_o$. In this way, a monoexponential decay with a lifetime of 1.9 ns was retrieved (Table 1). In addition, the fact that a biexponential decay, typical of a gel/fluid coexistence situation was also retrieved indicates that the $l_d$-enriched areas are probably not pure $l_d$, but contain a fraction of gel that cannot be resolved in the imaging methodologies. This could only be concluded by using the fixed laser beam configuration in the microscope, which retrieves high count fluorescence decays of Rhod-DOPE from different regions of the same GUV.

With the information collected in the present work it is possible to add information to the previously published phase diagram for the system DOPC/DPPC/cholesterol (27), in which only the $l_d/l_o$ phase coexistence region was depicted. Taking into account that:

1. The $l_d/l_o$ borders obtained by fluorescence microscopy shown in that diagram are at room temperature (24°C);
2. The fact that for DOPC/DPPC (1:1) mixtures with 9 and 12 mol % cholesterol and (3:7) mixtures with 9 mol % cholesterol, the three phases are present, as we show above in this study;
3. That the $l_o/s_o$ boundary for DPPC/cholesterol is between 7 and 28 mol % cholesterol (this work, Fig. 3 and (26,41,42)); and
4. The previously published binary gel/fluid DOPC/DPPC boundaries (22,23), the complete phase diagram for the DOPC/DPPC/cholesterol ternary system should be very close to that present in Fig. 6, with four regions of phase coexistence, as indicated.

Due to the restrictions imposed to the shape of the phase diagram by these results (points 1–4) and by the fact that two tie-lines of the same phase coexistence region can never cross, and considering the minimum angle between the $l_d/l_o$ and the $l_d/s_o$ quasi tie-lines sides of the tie-triangle (region 2), the uncertainty of the $l_d/l_o$ tie-line directions previously presented in Veatch et al. (27) crossing the 1:1:1 composition (region 1) can be further reduced. It is closer to the direction presented in that work for which the variation in cholesterol mole fraction is more pronounced, due to the exclusion of one of the possible tie-lines, as indicated in Fig. 6.

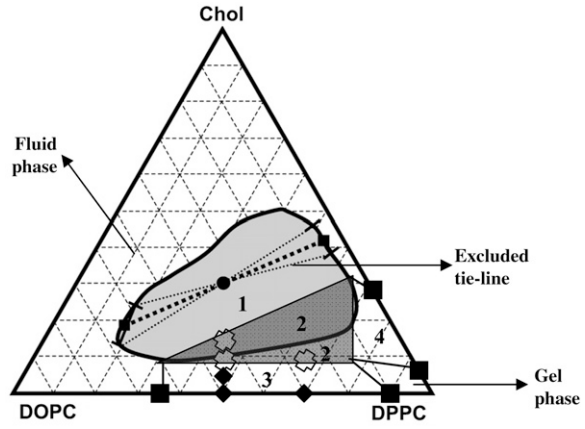


FIGURE 6 Ternary phase diagram for the DOPC/DPPC/cholesterol ternary lipid, raftlike system, at room temperature (24°C). The light-shaded area (region 1) indicates the $l_d/l_o$ phase coexistence, and was taken from Veatch et al. (27), which is in very good agreement with the data of the present work, except for a small portion of these area that corresponds to a three-phase coexistence situation, i.e., it is superimposed with the tie-triangle (region 2; see below). The solid squares indicate the gel/fluid ($l_d$) phase coexistence limits for the binary DOPC/DPPC mixture (22,23) at the bottom of the Gibbs triangle, and the gel/$l_o$ phase coexistence limits for the binary DPPC/cholesterol mixture ((24,41,42), and present work: see Fig. 3) at the right side of the Gibbs triangle. The latter ones and thermodynamic restrictions helped defining the gel/$l_o$ phase coexistence area (region 4). The solid diamonds correspond to binary or ternary lipid mixtures studied in the present work where only gel/$l_d$ phase coexistence was observed, and together with the gel/$l_d$ coexistence limits for the DOPC/DPPC binary system (*solid squares* at the bottom of the phase diagram) they define the gel/$l_d$ phase coexistence area (region 3). and the crosses correspond to compositions where three phases ($l_d$, $l_o$, and gel) were observed. From the latter points, a tie-triangle (limiting the three-phase coexistence area) was drawn with the minimal angle between the $l_d/l_o$ and $l_d$/gel sides that is possible in agreement with the experimental data: shaded area (region 2). Considering thermodynamic restrictions to the orientation of the tie-lines (8), the uncertainty in the $l_d/l_o$ tie-line that contains the 1:1:1 DOPC/DPPC/cholesterol equimolar mixture presented in Veatch et al. (27) can be reduced to the interval between the solid line and the dashed line with higher slope, i.e., that indicates a larger difference in cholesterol content between $l_d$ and $l_o$ phases (one of the possible tie-lines can be excluded by the present results, as indicated).

## Unraveling heterogeneity II: multiparameter approach

From recent fluorescence spectroscopy studies on membrane domains, it has become clear that the full characterization of binary and higher-order biologically relevant lipid systems

demands a multiprobe and multiparameter approach (37,48). In fluorescence lifetime image analysis there is often no statistical improvement in fitting the data to a biexponential model as compared to a monoexponential model. This is due to the small number of channels and low number of photon counts per pixel as compared to microscopic (using the fixed position laser beam) and macroscopic fluorescence decay analysis. In Figs. 1 and 5, the fluorescence decay in each pixel was analyzed with a single-exponential model, which means that information about possible multiexponential behavior is lost. However, if one of the fluorescence decay's components is independent of sample composition (within a limited uncertainty interval), this component can be fixed in the analysis, and an additional floating component can be added to the model. Because the fixed component is always present, it can be readily separated in this type of analysis, and a multiexponential behavior can be more easily discerned, even for the small count number decays of each pixel of a FLIM image. In this way, new parameters can be obtained: the preexponentials ($\alpha_1 + \alpha_2 = 1$), the fraction of light associated to each component, $F_i = \alpha_i\tau_i/\Sigma_i\alpha_i\tau_i$, and also the value of the second component lifetime $\tau_2$. Fixing one component in the image analysis is a common methodology when studying protein-protein interaction by FRET-FLIM. The occurrence of efficient fluorescence resonance energy transfer (FRET) between, for example, a CFP-tagged protein, and a putative interacting partner, YFP-tagged, will reveal if these molecules have a significant interaction in vivo. FRET will decrease the lifetime-weighted quantum yield of the donor, and this will be revealed in the lifetime image by pixels of a color corresponding to lower lifetimes than that of the image in a sample with donor alone, and also by the lifetime histogram. However, the noninteracting donor molecules, even in the samples with acceptor, retain their original fluorescence lifetime. In this way, it is common to analyze the image with a biexponential model, in which one of the lifetime components is fixed to the value of the donor in the absence of acceptor (39,49). Here, the same approach was employed to our previous data of Fig. 1 *J*. In the present study of lateral lipid heterogeneity, for the case of gel/fluid mixtures, a component of ~2.7 ns is always present, as shown by the microscopic and macroscopic decays (Tables 1 and 2). This motivated a biexponential analysis where one of the components was fixed to 2.7 ns and the other is allowed to float. In Fig. 7, an example is shown how images for the different parameters can be obtained from the same scan with this type of analysis, containing complementary information about the system and highlighting structural details. In fact, it can be seen that, for example, the blue area in Fig. 7 *B* ($F_1$ image) is divided in blue and green in Fig. 7 *C* ($\tau_2$ image). Furthermore, the distribution corresponding to $\tau_2$ is very interesting. The most prominent feature is the peak at ~2.4 ns. Above 2.5 ns, it is very close to the fixed 2.7 ns component. It corresponds to regions where the decay is close to monoexponential, and has a negligible contribution to the total decay, because dark blue regions can hardly be seen in Fig. 7 *C*. However, most of the peak corresponds to regions with a component slightly shorter than the fixed component (note that the distribution histogram for the pure components—Fig. 1, *C* and *F*—has null frequency below ~2.3 ns, and the peak in Fig. 7 *D* ends at ~2.0 ns). A shorter component of ~1.4–1.8 ns is now resolved, and this component is in very good agreement with the short component observed in the macroscopic decays for this mixture (Table 2), underlining the statistical and physical significance of this type of analysis. This analysis, together with the previous characterization of the probe photophysics, also reinforces that the variations of fluorescence lifetime observed arise from different probe concentrations in different phases. Hence, the complex patterns

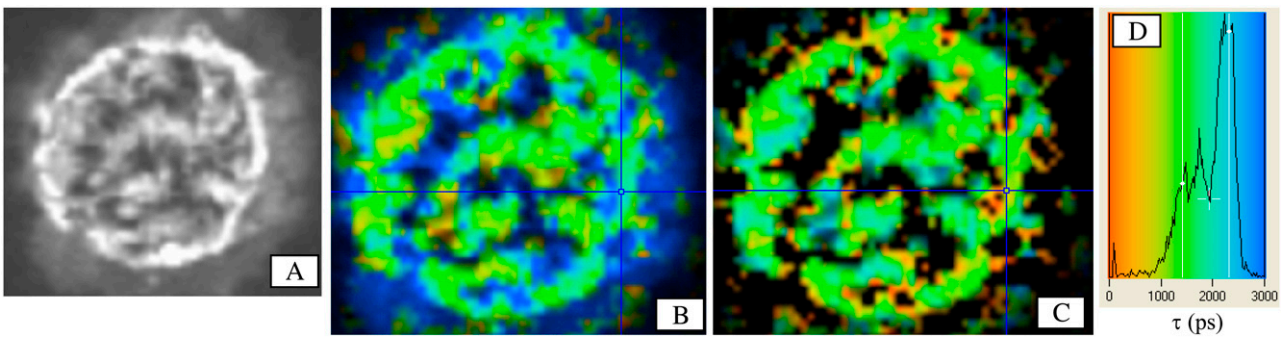


FIGURE 7 Application of a biexponential model to the FLIM data of a GUV composed of DOPC/DPPC in a 1:1 mol ratio + 12 mol % cholesterol, labeled with 0.2 mol % Rhod-DOPE, at room temperature (24°C). The data is the same that was used to make the image in Fig. 1 *K*. The fluorescence intensity image is given again now in panel *A*. A biexponential model (Eq. 1) was used to analyze the pixel decays. One of the components ($\tau_1$) was fixed to 2.7 ns, and the other component ($\tau_2$) was allowed to float. From this analysis different images can be generated: the fraction of emitted light corresponding to component 1 ($F_1 = \alpha_1\tau_1/(\alpha_1\tau_1 + \alpha_2\tau_2)$) leads to the image in panel *B* (the color code is from *red* ($F_1 = 0$) to *dark blue* ($F_1 = 1$)). The value of $\tau_2$ leads to the image in panel *C*, and the distribution histogram with the respective code color is given in panel *D*. The peak for very low value of $\tau_2$ (<0.3 ns) giving rise to red dots in panel *C* corresponds to pixels where the fraction of light associated to component 1 of the decay is close to 100% (*B*, *dark blue areas*), i.e., component 2 has no physical meaning in those pixels, and its contribution to the average lifetime and lifetime-weighted quantum yield is negligible.

observed in the different panels of Fig. 7 must originate from the different probe partition between the phases and from the domain interfaces.

## CONCLUSIONS AND FUTURE DEVELOPMENTS

In this work, for the first time, a combination of microscopic and macroscopic time-resolved fluorescence spectroscopy was applied to study lipid domains and rafts in different types of lipid vesicles. The approach involved a stepwise methodology that starts with the thorough characterization of the simpler systems, and where the complexity of the lipid mixtures is progressively increased. This approach resulted in interesting conclusions about binary and ternary mixtures of phospholipids and cholesterol.

Several lines of evidence point to a substructure of the domains visualized by two-photon microscopy, namely, extensive domain interfaces with significant probe partition, and fluorescence decay attributable to a gel/fluid phase coexistence corresponding to bright homogeneous areas in the intensity image. These results imply that:

1. There are limitations of two-photon and confocal microscopy to determine (quantitative) lipid phase diagrams, and consequently to quantify probe partitioning, quantum yield ratios among phases, and phase mole fractions, which is a direct result of the substructure of the domains that is not resolved in the image;
2. Other recent combined approaches are very important (e.g., (19,20,50,51)) in the study of membrane lipid domains;
3. The application of the fluorescence decay components to identify lipid phases can only be performed after a very careful characterization of the system in well-defined regions of the phase diagram; and
4. The combination of imaging methodologies with acquisition of high count number microscopic and macroscopic fluorescence decays are required for correct interpretation of complex lifetime image analysis.

The application of this approach revealed other features of membrane lateral organization, such as the clear identification of three-phase coexistence with a concomitant unambiguous attribution of the phases. Further developments of this approach will include the use of other probes (dual-color FLIM), FRET-FLIM, time-resolved fluorescence anisotropy imaging (see, for example, (52)), and finally, the study of lipid domains and rafts on cellular membranes. Potentially useful probes are lyso-Rhodamine-PE and octadecyl-Rhodamine, because they incorporate more readily in membranes and are sensitive to the presence of cholesterol-enriched domains. However, for the interpretation of results in more complex systems, like cell membranes, a previous characterization of the probe photophysics and of the instrument limitations of the methodology in well-defined systems, such as the one described in this work, will be essential.

This work and research were supported by the POCI, Fundação para a Ciência e a Tecnologia, Portugal (No. BPD/17842 to R.F.M. de A. and No. BPD/11488 to A.F., and project No. POCTI/QUI/57123/2004-2008) and by the Council for Earth and Life Sciences of The Netherlands Organization for Scientific Research (A.J.W.G.V.).

## REFERENCES

1. Mukherjee, S., and F. R. Maxfield. 2004. Membrane domains. *Annu. Rev. Cell Dev. Biol.* 20:839–866.
2. Kusumi, A., C. Nakada, K. Ritchie, K. Murase, K. Suzuki, H. Murakoshi, R. S. Kasai, J. Kondo, and T. Fujiwara. 2005. Paradigm shift of the plasma membrane concept from the two-dimensional continuum fluid to the partitioned fluid: high-speed single-molecule tracking of membrane molecules. *Annu. Rev. Biophys. Biomol. Struct.* 34:351–354.
3. Simons, K., and E. Ikonen. 1997. Functional rafts in cell membranes. *Nature.* 387:569–572.
4. Anderson, R. G. W., and K. Jacobson. 2002. Cell biology: A role for lipid shells in targeting proteins to caveolae, rafts, and other lipid domains. *Science.* 296:1821–1825.
5. London, E. 2002. Insights into lipid raft structure and formation from experiments in model membranes. *Curr. Opin. Struct. Biol.* 12: 480–486.
6. Edidin, M. 2003. Lipids on the frontier: a century of cell-membrane bilayers. *Nat. Rev. Mol. Cell Biol.* 4:414–418.
7. McMullen, T. P. W., R. N. A. H. Lewis, and R. N. McElhaney. 2004. Cholesterol-phospholipid interactions, the liquid-ordered phase and lipid rafts in model and biological membranes. *Curr. Opin. Colloid Interface Sci.* 8:459–468.
8. de Almeida, R. F. M., A. Fedorov, and M. Prieto. 2003. Sphingomyelin/phosphatidylcholine/cholesterol phase diagram: boundaries and composition of lipid rafts. *Biophys. J.* 85:2406–2416.
9. de Almeida, R. F. M., L. M. S. Loura, A. Fedorov, and M. Prieto. 2005. Lipid rafts have different sizes depending on membrane composition: a time-resolved fluorescence resonance energy transfer study. *J. Mol. Biol.* 346:1109–1120.
10. Silvius, J. R., and I. R. Nabi. 2006. Fluorescence-quenching and resonance energy transfer studies of lipid microdomains in model and biological membranes. *Mol. Membr. Biol.* 23:5–16.
11. Kahya, N., D. Scherfeld, K. Bacia, B. Poolman, and P. Schwille. 2003. Probing lipid mobility of raft-exhibiting model membranes by fluorescence correlation spectroscopy. *J. Biol. Chem.* 278:28109–28115.
12. Veatch, S. L., and S. L. Keller. 2005. Miscibility phase diagrams of giant vesicles containing sphingomyelin. *Phys. Rev. Lett.* 94:148101.
13. Veatch, S. L., and S. L. Keller. 2005. Seeing spots: complex phase behavior in simple membranes. *Biochim. Biophys. Acta Mol. Cell Res.* 1746:172–185.
14. Simons, K., and W. L. C. Vaz. 2004. Model systems, lipid rafts and cell membranes. *Annu. Rev. Biophys. Biomol. Struct.* 33:269–295.
15. Korlach, J., P. Schwille, W. W. Webb, and G. W. Feigenson. 1999. Characterization of lipid bilayer phases by confocal microscopy and fluorescence correlation spectroscopy. *Proc. Natl. Acad. Sci. USA.* 96: 8461–8466.
16. Dietrich, C., L. A. Bagatolli, Z. N. Volovyk, N. L. Thompson, M. Levi, K. Jacobson, and E. Gratton. 2001. Lipid rafts reconstituted in model membranes. *Biophys. J.* 80:1417–1428.
17. Kahya, N., and P. Schwille. 2006. Fluorescence correlation studies of lipid domains in model membranes. *Mol. Membr. Biol.* 23:29–39.
18. Ruan, Q., M. A. Cheng, M. Levi, E. Gratton, and W. W. Mantulin. 2004. Spatial-temporal studies of membrane dynamics: Scanning fluorescence correlation spectroscopy (SFCS). *Biophys. J.* 87:1260–1267.
19. Veatch, S. L., K. Gawrisch, and S. L. Keller. 2006. Closed-loop miscibility gap and quantitative tie-lines in ternary membranes containing diphytanoyl PC. *Biophys. J.* 90:4428–4436.

20. Chiantia, S., N. Kahya, J. Ries, and P. Schwille. 2006. Effects of ceramide on liquid-ordered domains investigated by simultaneous AFM and FCS. *Biophys. J.* 90:4500–4508.

21. Fidorra, M., L. Duelund, C. Leidy, A. C. Simonsen, and L. A. Bagatolli. 2006. Absence of fluid-ordered/fluid-disordered phase coexistence in ceramide/POPC mixtures containing cholesterol. *Biophys. J.* 90:4437–4451.

22. Lentz, B. R., Y. Barenholz, and T. E. Thompson. 1976. Fluorescence depolarization studies of phase transitions and fluidity in phospholipid bilayers. 2. Two component phosphatidylcholine liposomes. *Biochemistry.* 15:4529–4537.

23. Elliott, R., K. Katsov, M. Schick, and I. Szleifer. 2005. Phase separation of saturated and mono-unsaturated lipids as determined from a microscopic model. *J. Chem. Phys.* 122:44904–44911.

24. Lentz, B. R., D. A. Barrow, and M. Hoechli. 1980. Cholesterol-phosphatidylcholine interactions in multilamellar vesicles. *Biochemistry.* 19:1943–1954.

25. Ipsen, J. H., G. Karlstrom, O. G. Mouritsen, H. Wennerstrom, and M. J. Zuckermann. 1987. Phase-equilibria in the phosphatidylcholine-cholesterol system. *Biochim. Biophys. Acta.* 905:162–172.

26. Vist, M. R., and J. H. Davis. 1990. Phase equilibria of cholesterol/dipalmitoylphosphatidylcholine mixtures: $^{2}$H nuclear magnetic resonance and differential scanning calorimetry. *Biochemistry.* 29:451–464.

27. Veatch, S. L., I. V. Polozov, K. Gawrisch, and S. L. Keller. 2004. Liquid domains in vesicles investigated by NMR and fluorescence microscopy. *Biophys. J.* 86:2910–2922.

28. Scherfeld, D., N. Kahya, and P. Schwille. 2003. Lipid dynamics and domain formation in model membranes composed of ternary mixtures of unsaturated and saturated phosphatidylcholines and cholesterol. *Biophys. J.* 85:3758–3768.

29. Bagatolli, L. A., and E. Gratton. 2000. Two photon fluorescence microscopy of coexisting lipid domains in giant unilamellar vesicles of binary phospholipid mixtures. *Biophys. J.* 78:290–305.

30. Mayer, L. D., M. J. Hope, and P. R. Cullis. 1986. Vesicles of variable sizes produced by a rapid extrusion procedure. *Biochim. Biophys. Acta.* 858:161–168.

31. Angelova, M. I., and D. S. Dimitrov. 1986. Liposome electroformation. *Faraday Discuss. Chem. Soc.* 81:303–311.

32. Estes, D. J., and M. Mayer. 2005. Electroformation of giant liposomes from spin-coated films of lipids. *Colloid Surf. B Biointerfaces.* 42:115–123.

33. Rodriguez, N., F. Pincet, and S. Cribier. 2005. Giant vesicles formed by gentle hydration and electroformation: a comparison by fluorescence microscopy. *Colloid Surf. B Biointerfaces.* 42:125–130.

34. McClare, C. W. 1971. An accurate and convenient organic phosphorus assay. *Anal. Biochem.* 39:527–530.

35. Haugland, R. 1996. Handbook of Fluorescent Probes and Research Chemicals. Molecular Probes, Eugene, OR.

36. De La Serna, J. B., J. Perez-Gil, A. C. Simonsen, and L. A. Bagatolli. 2004. Cholesterol rules: direct observation of the coexistence of two fluid phases in native pulmonary surfactant membranes at physiological temperatures. *J. Biol. Chem.* 279:40715–40722.

37. de Almeida, R. F. M., M. A. Hink, J. W. Borst, M. Prieto, and A. J. W. G. Visser. 2006. Lipid domains and rafts studied by time-resolved fluorescence microspectroscopy. *In* Biochemistry and Biophysics of Lipids. A. Pramanik, editor. Transworld Research Network, Kerala, India.

38. Becker, W., A. Bergmann, M. A. Hink, K. Konig, K. Benndorf, and C. Biskup. 2004. Fluorescence lifetime imaging by time-correlated single-photon counting. *Microsc. Res. Tech.* 63:58–66.

39. Borst, J. W., M. A. Hink, A. Van Hoek, and A. J. W. G. Visser. 2003. Multiphoton microspectroscopy in living plant cells. *Proc. SPIE.* 4963: 231–238.

40. Loura, L. M. S., A. Fedorov, and M. Prieto. 2001. Fluid-fluid membrane microheterogeneity: a fluorescence resonance energy transfer study. *Biophys. J.* 80:776–788.

41. McMullen, T. P. W., and R. N. McElhaney. 1995. New aspects of the interaction of cholesterol with dipalmitoylphosphatidylcholine bilayers as revealed by high-sensitivity differential scanning calorimetry. *Biochim. Biophys. Acta Biomembr.* 1234:90–98.

42. Sankaram, M. B., and T. E. Thompson. 1991. Cholesterol-induced fluid-phase immiscibility in membranes. *Proc. Natl. Acad. Sci. USA.* 88:8686–8690.

43. Thewalt, J. L., and M. Bloom. 1992. Phosphatidylcholine—cholesterol phase-diagrams. *Biophys. J.* 63:1176–1181.

44. MacDonald, R. I. 1990. Characteristics of self-quenching of the fluorescence of lipid-conjugated rhodamine in membranes. *J. Biol. Chem.* 265:13533–13539.

45. Silva, L., R. F. M. de Almeida, B. M. Castro, A. Fedorov, and M. Prieto. 2007. Ceramide-domain formation and collapse in lipid raft membranes: membrane reorganization induced by an apoptotic lipid. *Biophys. J.* 92:502–515.

46. Blackman, M. J., J. E. T. Corrie, J. C. Croney, G. Kelly, J. F. Eccleston, and D. M. Jameson. 2002. Structural and biochemical characterization of a fluorogenic rhodamine-labeled malarial protease substrate. *Biochemistry.* 41:12244–12252.

47. Reference deleted in proof.

48. Silva, L., R. F. M. de Almeida, A. P. Matos, A. Fedorov, and M. Prieto. 2006. Ceramide-platform formation and -induced biophysical changes in a fluid phospholipid membrane. *Mol. Membr. Biol.* 23:305–315.

49. Snippe, M., J. W. Borst, R. Goldbach, and R. Kormelink. 2005. The use of fluorescence microscopy to visualize homotypic interactions of Tomato Spotted Wilt Virus nucleocapsid protein in living cells. *J. Virol. Methods.* 125:15–22.

50. Korlach, J., T. Baumgart, W. W. Webb, and G. W. Feigenson. 2005. Detection of motional heterogeneities in lipid bilayer membranes by dual probe fluorescence correlation spectroscopy. *Biochim. Biophys. Acta Biomembr.* 1668:158–163.

51. Coste, V., N. Puff, D. Lockau, P. J. Quinn, and M. I. Angelova. 2006. Raft-like domain formation in large unilamellar vesicles probed by the fluorescent phospholipid analogue, C12NBD-PC. *Biochim. Biophys. Acta Biomembr.* 1758:460–467.

52. Sharma, P., R. Varma, R. C. Sarasij, I. K. Gousset, G. Krishnamoorthy, M. Rao, and S. Mayor. 2004. Nanoscale organization of multiple GPI-anchored proteins in living cell membranes. *Cell.* 116:577–589.